Conformationally Constrained Peptides with High Affinity to the Vascular Endothelial Growth Factor

Ivan Guryanov,[1]* Viktor Korzhikov-Vlakh[1], Madhushree Bhattacharya[3], Barbara Biondi[2], Giulia Masiero[2], Fernando Formaggio[2], Tatiana Tennikova[1], and Arto Urtti[3]

[1]*Institute of Chemistry, St. Petersburg State University, St. Petersburg, Peterhof, Russia*

[2]*ICB, Padova Unit, CNR, Department of Chemistry, University of Padova, Padova, Italy*

[3]*Centre for Drug Research, Division of Pharmaceutical Biosciences, University of Helsinki, Helsinki, Finland*

ABSTRACT: The design of efficient vascular endothelial growth factor (VEGF) inhibitors is a high-priority research area aimed at the treatment of pathological angiogenesis. Among other compounds, v114* has been identified as a potent VEGF-binding peptide. In order to improve the affinity to VEGF, we built a conformational constrain in its structure. To this aim, Cα-tetrasubstituted amino acid Aib was introduced into the N-terminal tail, peptide loop, or C-terminal helix. NMR studies confirmed the stabilization of the helical conformation in proximity to the Aib residue.

We found that the induction of the N-terminal helical structure or stabilization of the C-terminal helix can noticeably increase the peptide affinity to the VEGF. These peptides efficiently inhibited VEGF-stimulated cell proliferation as well. The insertion of the non-proteinogenic Aib residue significantly enhanced the stability of the peptides in the vitreous environment. Thus, these Aib-containing peptides are promising candidates for the design of VEGF inhibitors with improved properties.

INTRODUCTION

The vascular endothelial growth factor (VEGF) is one of the main regulators of the angiogenesis.1 Unregulated expression of this protein causes proliferation and migration of the endothelial cells and uncontrolled growth of microvessels in various tissues (pathological angiogenesis). This phenomenon contributes to the pathogenesis of a number of diseases, such as tumor growth, psoriasis, arthritis, and age-related macular degeneration (AMD).2 The main reason of the wet form of AMD is the VEGF-dependent increase in vascular permeability and retinal pigment epithelial

detachment, which accounts for over 90% of the cases with severe visual loss with many complications, such as subretinal and vitreous hemorrhage, fibrosis, and scarring.3 The number of patients with AMD is expected to reach 288 millions worldwide in 2040.4 Though noticeable advances in AMD treatment have been achieved over the last years, the development of novel and improved therapeutic strategies remains highly requested.

There are various possibilities to control the activity of VEGF-dependent signaling pathways: inhibition of the endogenous secretion of the VEGF; neutralization of the VEGF with oligonucleotides, antibodies, and VEGF-binding extracellular receptor domains; and the use of low-molecular- weight inhibitors of the VEGF receptor interaction.5,6 Among the compounds developed so far, antibodies and soluble receptors (decoy receptors) are the most widespread in AMD therapy. Bevacizumab (Avastin), ranibizumab (Lucentis), and pegaptanib (Macugen) injections have been used extensively in ophthalmology for AMD, diabetic retinopathy, retinal vein occlusions, retinopathy of prematurity, and other chorioretinal vascular disorders.[7] The full-length soluble receptor is currently used in medicine with the name aflibercept (Eylea). Many attempts were made to design VEGF inhibitors based only on the binding domains of the receptor for the vascular endothelial growth factor (VEGFR), such as VEGF- trap (Regeneron Pharmaceuticals, Inc), a chimeric fusion molecule consisting of the second Ig domain of VEGFR-1 and the third domain VEGFR-2 fused to the Fc portion of IgG1.[8] Despite all the achievements in the treatment of AMD, the design of novel VEGF inhibitors remains a high-priority research area since many drawbacks are associated with the current pharmaceuticals. The anti-VEGF injections are given as a long-term treatment and constitute a significant burden for both patients and medical personnel. The fast elimination from the vitreous, suboptimal dosing frequency, and the risk of complications, such as endophthalmitis, uveitis, and vitreous hemorrhage, limit the use and the patient compliance of the existing antiangiogenic therapy.[9] Effective long-acting and/or minimally invasive drug delivery would noticeably improve ophthalmologic therapy. Furthermore, as a significant fraction of the patient population responds poorly, new pharmaceutical options are needed.

From this point of view, the design of small peptide VEGF inhibitors can be a promising approach for the development of novel pharmaceuticals with enhanced binding activity and stability for the treatment of VEGF-dependent diseases, including AMD.10,11 Several short peptides, which could interact with the VEGFR-binding surface of the VEGF with high affinity and selectivity, have been described.12,13 In particular, two promising cyclic helical anti-VEGF peptides v107 (GGNEc[CDIARMWEWEC]FERL) and v114 (VEPNc[CDIHVMWEWEC]FERL) with KD values of 0.53 and 0.11 μM, respectively, were identified by the phage display technique. V114*, in which the methionine residue was replaced by norleucine, was able to inhibit the VEGF with a Ki as low as 60 nM (competitive fluorescence polarization assay). Alanine scans of v107 and v114 and "β-scan" of v114* revealed the sites in their sequences involved in the interaction with the VEGF.[14]

Despite extensive studies on peptidomi- metics based on v114*, molecules with increased affinity and improved VEGF inhibition properties have not been identified so far. However, it was concluded that the reduction of its conformational freedom and the introduction of fluorination patterns to Phe16 may improve VEGF binding.[15]

In this study, we introduced an α-aminoisobutyric acid (Aib) residue into the amino acid sequence of v114* in order to reduce the flexibility of the peptide. Aib, as well as many other Cα-tetrasubstituted α-amino acids, is known to promote highly rigid and well-developed folded structures even in the short peptides.[16−21] The creation of such a conformational constraint can be particularly useful in the case of the helical peptide v114*. Moreover, the insertion of the non- proteinogenic Aib residue may increase the resistance to enzymatic degradation. Indeed, Aib has already been successfully exploited for the creation of several peptide drugs, such as semaglutide and abaloparatide.[22,23]

RESULTS AND DISCUSSION

We introduced the Aib residue in those sites of the v114* sequence which are not involved in the direct interaction with the VEGF and are not crucial for its binding. Previously, it was shown that v107 is strikingly amphipathic, and in the complex with the VEGF, it adopts a mixed conformation with the disordered N-tail (residues 1−4), type-I β-turn (residues 6−9), extended region (residues 9−12), and C-terminal α-helix (residues 13−19) Hydrophobic Ile7, Ala8, Met10, Trp11, Trp13, Phe16, and Leu19 are situated at the interface with the VEGF molecule (Figure 1).[24]

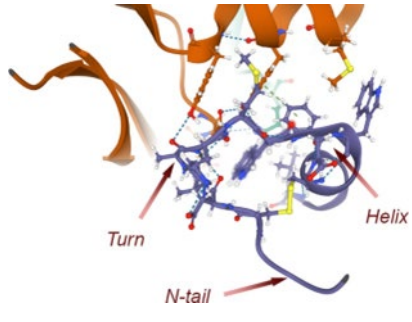

Figure 1. Structure of v107 in the VEGF-bound state and the sites in the peptide sequence suitable for Aib insertion (PDB: 1KAT).

The similarity of the amino acid sequences of v107 and v114* allows for supposing a resemblance of their con- formation in the bound state. Therefore, for the modification, we selected positions 8 and 12, where turn or helix rigidity, respectively, can increase the affinity to the VEGF (entries 3 and 4, Table 1).

Table 1. Amino Acid Sequences of v114* Analogues

entry	abbreviation	structure
1	v114*	VEPNc[CDIHV^{n}LWEWEC]FERL
2	Aib2	VAibPNc[CDIHV^{n}LWEWEC]FERL
3	Aib8	VEPNc[CDIAibV^{n}LWEWEC]FERL
4	Aib12	VEPNc[CDIHV^{n}LWAibWEC]FERL
5	kv114*	KAibKKc[CDIHV^{n}LWEWEC]FERL
6	sv114*	c[CDIHV^{n}LWEWEC]FERL
7	VN	VNc[CDIHV^{n}LWEWEC]FERL

We also studied the effects of N-terminal shortening (entry 6, Table 1) and Aib insertion into the N-terminal tail (entry 2, Table 1) on peptide rigidity and VEGF binding. We have recently shown that the modification of the peptides with a short oligolysine sequence is a useful method for their non-covalent attachment and retention on the negatively charged surfaces of nanoparticles covered by a heparin layer.[25] Oligolysines can also enhance the binding of the peptides to the negatively charged cell surface and increase the elimination of the complex peptide/complementary ligand from the extracellular space by endocytosis. Here, we extended this approach to the synthesis of anti-VEGF peptides. To this aim, along with the introduction of Aib, we substituted three N- terminal amino acids of v114* with lysines, which could also slow down the elimination of the peptide from the vitreous humor due to the interaction with negatively charged hyaluronic acid of the vitreous (Table 1, entry 5).

The preparation of the Aib-containing peptides is known to be rather complicated because of the steric hindrance of Aib. Therefore, the activation of its carboxylic group requires more efficient reagents than those commonly used. Thus, we introduced several modifications to the previously described procedure for the synthesis of Aib-containing analogues of v114*.[14,15] In particular, Aib and the following amino acid were coupled by means of HATU instead of HBTU, which allowed completion of the reaction with good yields. Interestingly, in the case of Aib2, a deletion peptide, where Aib and Pro are lacking (peptide VN, Table 1), was separated as a main product. The inherent propensity of the -Aib-Pro- motif to form a *β*-turn and the easiness by which Pro adopts a *cis* amide bond promoted the well-known intramolecular cyclization to diketopiperazine upon Fmoc-cleavage from Aib with piperidine (Figure S1).[26–28] In order to suppress this side reaction, Fmoc-removal was carried out in the presence of OxymaPure, which is able to protonate the forming amino group and, therefore, to decrease its nucleophilicity.[29] Thus, after cleavage of the peptide from the solid support and cyclization by air oxidation in a basic aqueous solution, the target peptide was obtained with a good yield and purity (Table S1 and Figure S2). However, the deletion peptide VN was also included in the further experiments in order to study the effect of the partial shortening of the N-terminal tail on the VEGF binding.

The 3D structures of the peptides were investigated by circular dichroism (CD) spectroscopy.[30] In the phosphate buffer (PBS) solution, the peptides adopted a mixed conformation, where the helix and random coil coexist, regardless of whether they contained Aib or not (Figure 2A).

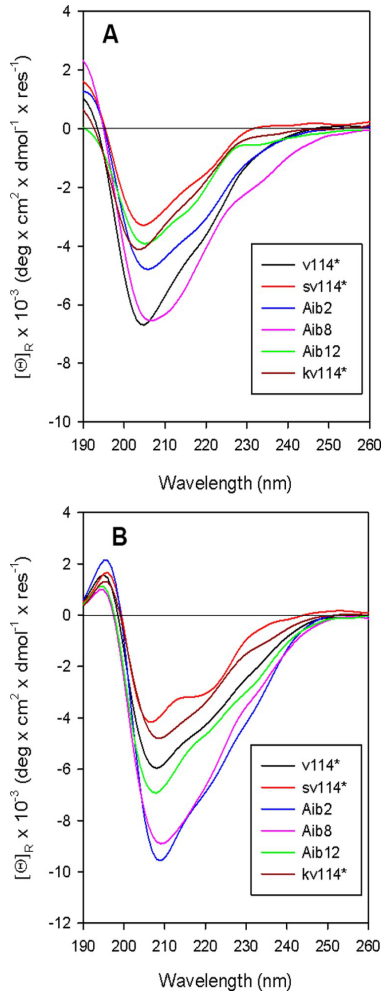

Figure 2. CD spectra of the peptides in PBS (A) and in methanol (B).

In methanol, the helical structure prevailed for all peptides (Figure 2B). Indeed, in this organic solvent, the negative $\pi \rightarrow \pi^*$ transition moves to longer wavelengths, close to the canonical 208 nm of the α-helix, and its negative maximum at 222 nm has a stronger intensity. Kv114*, if compared to Aib2, had a lower tendency to assume the helical conformation, even if it had Aib in the same position. This is probably related to the repulsion of the three protonated N-terminal lysines.

Contrary to CD spectroscopy, 2D-NMR allows us to assign the conformation of each individual peptide segment. Thus, more detailed information on the structure of the peptides was obtained from a 2D-NMR analysis. The fingerprint region of the nuclear Overhauser effect spectroscopy (NOESY) spectrum of v114* in the unbound state showed $C^{\alpha}H_i \rightarrow NH_{i+2}$, $C^{\alpha}H_i \rightarrow NH_{i+3}$ and $C^{\alpha}H_i \rightarrow NH_{i+4}$ cross-peaks from Cys5 to Phe16. The interactions Asp6/His8 and Cys5/Val9, as well as the signal arising from the proximity of Cys5 and Trp11, can be attributed to the formation of the

loop at this peptide segment, followed by the C-terminal helix, the presence of which is evidenced by the interactions Trp13/ Phe16 and Glu14/Glu12. No proton correlations were observed in the N-terminal part of the peptide (Figure 3A).

Furthermore, the amide proton region exhibited the cross- peaks characteristic of a helical conformation, which extended toward the C-terminal end of the peptide (Figure S6). This is in agreement with the literature data[24] and confirms the similarity of the spatial conformations of v107 and v114*.

The introduction of Aib into the amino acid sequence of the parent peptide v114* drastically changed its secondary structure. The fingerprint region of the NOESY spectrum of Aib2 highlighted medium-range correlations typical of the α- helix not only in the C-terminal part but also in the N-terminal tail, starting from Val at position 1 (Figure 3B). A similar pattern was also evident in the aliphatic/NH region, where a $C^{\beta}H_i \rightarrow NH_{i+4}$ correlation between Aib2 and Asp6 was observed along with the Aib2/Cys5 $C^{\beta}H_i \rightarrow NH_{i+3}$ cross-peak (Figure S10). At the same time, the fingerprint region of the peptide loop in the NOESY spectrum noticeably changed with the appearance of the signals due to the $C^{\alpha}H_i \rightarrow NH_{i+3}$ interactions Cys5/Ile7, Asp6/Val9, Asp6/Nle10, and Nle10/ Glu12 and the disappearance of the long-range cross-peak Cys5/Trp11, probably because of the involvement of the Cys5 residue in the helix. Thus, the helix-promoting influence of the Aib2 residue extends up to the N-terminal part of the loop and, apparently, changes the conformation of its C-terminal portion to maintain the cyclic peptide structure.

The NOESY spectrum of Aib8 showed that the C^{α}- tetrasubstituted Aib residue involved in the helical conforma- tion was in the central part of the peptide loop but maintained the vicinity of Cys5 to Trp11 similar to the parent peptide v114* (Figure 3C). In the aliphatic/NH region of the NOESY spectrum, we observed medium-range correlations from Aib8 to Glu12: two $C^{\beta/\gamma}H_i \rightarrow NH_{i+3}$ (Aib8/Trp11 and Val9/Glu12) correlations and a $C^{\beta}H_i \rightarrow NH_{i+4}$ (Aib8/Glu12) cross-peak (Figure S14). Moreover, the helix-promoting effect of Aib was also seen in the N-terminal part of the peptide with the appearance of the signal due to the vicinity of Asn4 to Aib8. Thus, Aib seems to induce a helical formation rather than a simple turn in the peptide loop.

In the fingerprint region of the NOESY spectrum of Aib12, a set of strong medium-range correlations from Ile7 to Cys15 could be identified. In particular, two $C^{\alpha}H_i \rightarrow NH_{i+3}$ (His8/ Trp11 and Nle10/Trp13) and two $C^{\alpha}H_i \rightarrow NH_{i+4}$ (Ile7/ Trp11 and Trp11/Cys15) cross-peaks could be seen (Figure 3D). A medium-range interaction between Ile7 and Trp11 was also observed in the aliphatic/NH region (Figure S18). The amide proton region contained most of the sequential $N{-}H_i \rightarrow N{-}H_{i+1}$ correlations in the region comprising the segment 9−19 of Aib12, suggesting the presence of a stable helical conformation in this region. Similar to Aib2, no signal due to the vicinity of Cys5 to Trp11 was found in this case because of the involvement of Trp11 in the helical structure and the influence of Aib that extended up to the C-terminal part of the peptide loop. However, an increase in the flexibility was observed for the N-terminal segment.

Thus, NMR data confirmed the conformational constraint induced by the presence of Aib in its adjacent regions. In particular, stabilization of helical structures was observed in the N-terminal and C-terminal segments of Aib2 and Aib12, respectively, with corresponding conformational changes of the peptide loop to maintain the overall cyclic peptide structure. Interestingly, in the case of Aib8, the insertion of Aib did not lead to an increase in the turn rigidity but promoted helix formation in the central part of the peptide.

To study the resistance of the peptides to the enzymatic degradation, stability in the vitreal environment was carried out by incubating the peptides in the porcine vitreous at 37 °C. The introduction of the non-proteinogenic amino acid into the structure of most peptides significantly increased their stability in comparison to that of the peptides containing only coded amino acids (Figure 4).

The lifetime of Aib-containing peptides in the porcine vitreous increased by 7−10 times, compared to that of the parent peptide v114*, with the only exception of Aib12, which disappeared after 10 days and showed to be less stable in solution than v114*.

Cytotoxicity of the peptides was evaluated by a 3-(4,5- dimethylthiazol-2-yl)-2,5-diphenyltetrazolium bromide (MTT) assay. Most of the peptides were not toxic to the ARPE-19 cells at concentrations up to 20 μM (Figure S19). These results confirm the potential of the Aib-containing analogues of v114* as promising anti-VEGF compounds.

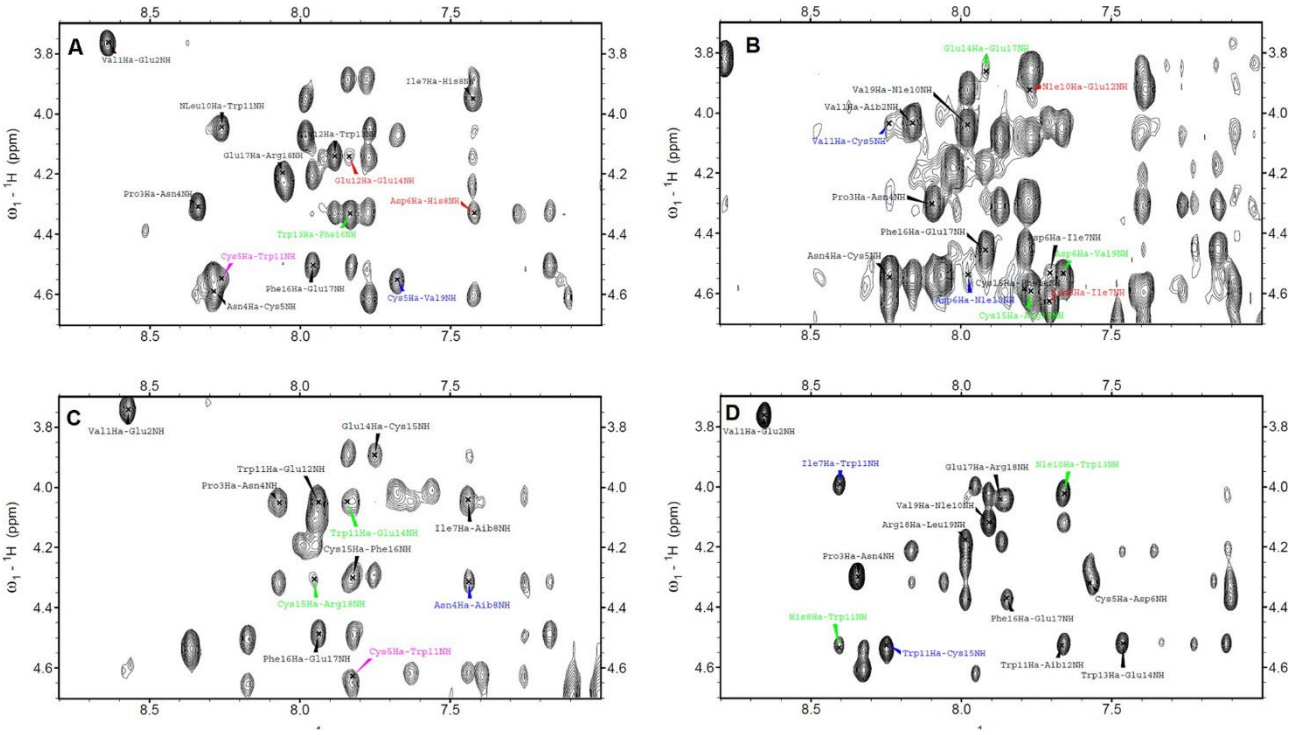

Figure 3. Fingerprint region of the NOESY spectra of v114* (A), Aib2 (B), Aib8 (C), and Aib12 (D). Medium-range interactions are highlighted in red (CαHi → NHi+2), green (CαHi → NHi+3), and blue (CαHi → NHi+4). The cross-peak due to the interaction Cys5/Trp11 is evidenced in magenta.

The affinity of the peptides to the VEGF was studied by means of microscale thermophoresis (MST) both immediately after peptide and protein mixing and after 30 min incubation of the peptide/VEGF mixture in order to reach the equilibrium state of the complex. MST data without incubation showed that complete removal of the N-terminal tail significantly reduced the ability of v114* to bind the VEGF (Table 2).

However, the elimination of only glutamic acid and proline (peptide VN) led to a 2-fold increase of the affinity. This observation evidences the influence of the N-terminal tail despite the absence of the direct interaction with the VEGF, which was shown by β^3-substitutions.[14] The introduction of Aib into the peptide sequence favored VEGF binding with a corresponding K_D decrease. This is in accordance with the hypothesis of Reille-Seroussi[15] about the importance of the conformational constraint for tight VEGF binding. However, in the case of histidine/Aib substitution at position 8, where the parent peptide adopts a turn conformation, the affinity to the VEGF decreased dramatically (entry 3, Table 2). Apparently, the formation of the rigid helical structure instead of the turn in the peptide loop prevented its interaction with the VEGF.

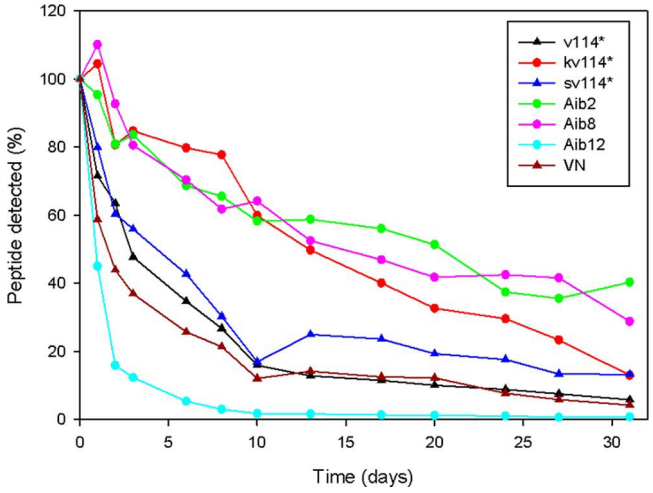

Figure 4. Peptide stability in the porcine vitreous. The peptides were incubated with the porcine vitreous, and the stability was determined by measuring their concentration at different time intervals using UPLC−MS/MS.

Table 2. Affinity of the Peptides to the VEGF

entry	compound	K_D, nM (no incubation)	K_D, nM (with incubation)
1	v114*	3870 ± 40	300 ± 75
2	Aib2	2970 ± 30	4 ± 1
3	Aib8	11800 ± 140	not determined
4	Aib12	940 ± 20	150 ± 4
5	kv114*	540 ± 20	3000 ± 263
6	sv114*	9970 ± 180	not determined
7	VN	1940 ± 40	not determined
8	bevacizumab	not determined	4 ± 1

The affinity of the Aib-containing peptides that showed the strongest VEGF binding was evaluated after the incubation of the mixture before carrying out the MST measurement. In most of the cases, a strong K_D decrease was observed. This can be due to the time necessary to the peptides to reach the binding site of the VEGF. However, in the case of kv114*, an opposite behavior was seen. Probably, the time-dependent decrease of the affinity is caused by a conformational rearrangement of the bound peptide and the repulsion of the positively charged N-terminal amino groups. On the contrary, Aib2 with a similar structure but without N-terminal lysines showed an affinity similar to those of bevacizumab with the K_D in the nanomolar range.

Though the MST technique was shown to be a powerful tool for the analysis of the binding affinities, it cannot be applied in the live systems, where multiple interactions with cells and cell components can take place, thus changing the physico-chemical and biological properties of the biomolecules under

study. Therefore, the results of the MST assay can differ from those obtained in the cell culture. In order to evaluate the VEGF signaling inhibition, the proliferation of VEGF-depend- ent human umbilical vein endothelial cells (HUVECs) in the presence of the peptides was studied. As a positive control, bevacizumab was taken also in this case (Figure 5, Table 3).

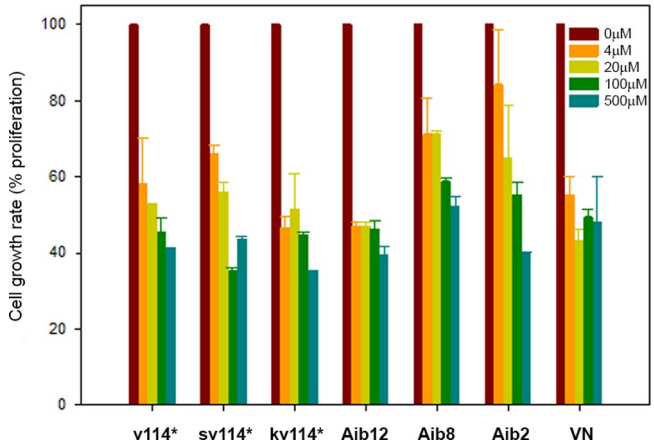

Figure 5. Inhibition of VEGF-induced proliferation of HUVEC cells in the presence of anti-VEGF peptides.

IC_{50} values for bevacizumab and v114* were 1 nM and 20 μM, respectively, which was in line with the results obtained by Haase et al.[14] The more potent VEGF inhibition by the monoclonal antibody can be explained by its larger VEGF binding surface than that of the peptides. As is in the case of the MST assay, Aib-containing analogues displayed higher VEGF-binding activity than the parent peptide v114*, with an exception of Aib8, where the constrained loop is, probably, responsible for the lower VEGF inhibition. VN with a shortened N-tail showed stronger VEGF binding than v114*. It confirmed the importance of N-terminal residues for the stabilization of the conformation necessary for the interaction with the VEGF molecule. However, the low enzymatic stability of this peptide and that of Aib12 reduce their potential as VEGF inhibitors. Interestingly, kv114* displayed stronger VEGF inhibition than Aib2 with a similar structure, probably due the interaction of the peptide or the peptide/VEGF complex with negatively charged cell surfaces or other cell culture components, as in the case of the oligolysine-containing chemokine inhibitors described in our previous work.[25] However, this phenomenon needs a more detailed inves- tigation by using, for example, fluorescently labeled peptides to study their distribution. Thus, among the peptides studied, conformationally constrained peptides Aib2 and kv114* showed both high stability in the porcine vitreous and strong VEGF binding, which proves their high potential for further development of efficient VEGF inhibitors.

Table 3. VEGF-Induced Proliferation of HUVECs in the Presence of the Peptides and Bevacizumab

entry	compound	IC_{50}, μM ± SD
1	v114*	20.0 ± 3.5
2	Aib2	10.0 ± 1.1
3	Aib8	50.0 ± 14.1
4	Aib12	3.5 ± 0.7
5	kv114*	6.0 ± 0.4
6	sv114*	12.0 ± 5.1
7	VN	4.0 ± 0.5
8	bevacizumab	$1 \times 10^{-3} \pm 0.086 \times 10^{-3}$

In summary, herein, we reported a series of cyclic peptides that contain C^{α}-tetrasubstituted amino acid Aib at different positions. The insertion of Aib into the structure of the parent peptide v114* generated a conformational constraint at the corresponding sites of the peptide sequence. We found that the induction of an N-terminal helical conformation or stabiliza- tion of the C-terminal helix could noticeably increase the affinity of these Aib-containing v114* analogues to the VEGF. In addition, the insertion of Aib significantly reduced the sensitivity of the peptides to the enzymatic degradation and enhanced their stability in the vitreous environment. Thus, these Aib-containing peptides are promising candidates for the design and development of the inhibitors with enhanced VEGF binding.

EXPERIMENTAL SECTION

Materials. Materials were purchased from the following: Iris Biotech: *N*,*N*-dimethylformamide (DMF), dichloromethane, *N*,*N*- diisopropylethylamine (DIPEA), trifluoroacetic acid (TFA), piper- idine, and Rink amide resin; Sigma Aldrich: acetonitrile for mass spectrometry (MS) (>99,9%), TFA for MS (>99,9%), diethyl ether, triisopropylsilane (TIS), Fmoc-Aib-OH, and ethanedithiol (EDT); Carbosynth: ethyl (hydroxyimino)cyanoacetate (OxymaPure), HBTU, and HATU; GL Biochem: Fmoc-Val-OH, Fmoc-Glu- (O*t*Bu)-OH, Fmoc-Pro-OH, Fmoc-Asn(Trt)-OH, Fmoc-Cys(Trt)- OH, Fmoc-Asp(O*t*Bu)-OH, Fmoc-Ile-OH, Fmoc-His(Trt)-OH, Fmoc-Nle-OH, Fmoc-Trp(N^{in}Boc)-OH, Fmoc-Phe-OH, Fmoc-Arg- (Pbf)-OHand Fmoc-Leu-OH.

Peptide Synthesis. The synthesis was carried out on an automatic peptide synthesizer Biotage SyroWave. Fmoc-protected Rink amide resin (250 mg; 0.65 mmol/g) was swelled in 2 mL of DMF for 30 min, the solvent was filtered off, and the Fmoc protective group was removed with 20% piperidine in DMF (two cycles for 5 and 20 min). Then, the resin was washed four times with 2 mL of DMF, and acylation was performed. At each acylation step (1 h), 5- fold excess of protected amino acid and HBTU and 7-fold excess of DIPEA were used. In the case of Aib and the following amino acid, the acylation was performed two times with 5 equivalents of HATU and 7 equivalents of DIPEA. After each acylation, the resin was washed three times with 2 mL of DMF. The cycles of acylation and Fmoc deprotection were repeated until the desired peptide sequences were obtained. In the case of Aib2, the Fmoc removal from Aib was carried out with a 20% piperidine solution containing 1M Oxy- maPure. At the end of the synthesis, the peptides were cleaved from the resin with 3 mL of the mixture of TFA/water/TIS/EDT (*v*/*v*/*v*/*v* 94/2.5/1/2.5) and precipitated in 5 mL of diethyl ether. The precipitate was centrifuged and

dried. The resulting linear peptide was dissolved in a 0.15M ammonium bicarbonate solution to a concentration of 1 mg/mL. The solution was stirred for several days until the disulfide bond formation reaction was complete [high- performance liquid chromatography−MS (HPLC−MS) monitoring]. Then, the pH of the resulting solution was adjusted to 2 with 1M hydrochloric acid, and the product was purified by preparative HPLC on an ÄKTA Pure purification system with UV detection at 224 nm using a C18 Jupiter column Phenomenex (21.2 × 250 mm) and eluent A: 10% acetonitrile in water with 0.1% TFA and eluent B: 90% acetonitrile in water with 0.1% TFA. Elution was carried out using the following gradient: 0 min□5% eluent B, 20 min□31% eluent B; 65 min□38% eluent B, and 70 min□95% eluent B. Fractions with a purity >97% were collected and lyophilized. The resulting peptides were analyzed by HPLC−MS (see the Supporting Information).

HPLC−MS Analyses. HPLC−MS analyses were performed on an Agilent Technologies 1200 instrument in tandem with an Agilent 6530 mass accuracy Q-ToF using a C18 Pore-shell column (4.6 × 100 mm). Analytical method: eluent A: TFA/H_2O 0.1% *v*/*v*; eluent B: TFA/MeCN 0.1% *v*/*v*; detection at 224 nm; and gradient elution: 0 min□10% eluent B, 3 min□10% eluent B, 33 min□95% eluent B, and 38 min□95% eluent B.

NMR Analysis. All NMR experiments were carried out at 298 K in a 9:1 (*v*/*v*) H_2O/D_2O mixture (peptide concentration 1.2 mM) using a Bruker AVANCE Neo spectrometer operating at 600 MHz and the TOPSPIN software package. Water suppression was obtained through excitation sculpting.[31] The homonuclear spectra were acquired by collecting 512 experiments consisting of 64−80 scans and 2000 data points. The spin systems of coded amino acid residues were identified using standard DQF-COSY and CLEAN-TOCSY spectra.[32−34] In the latter case, the spin-lock pulse sequence was 70 ms long. NOESY experiments were utilized for sequence-specific assignment.[35] At the beginning of the experiments, the build-up curve of the volumes of NOE cross-peaks as a function of the mixing time (50−500 ms) was obtained in order to avoid the problem of spin diffusion. The mixing time of the NOESY experiment used for interproton distance determination was 150 ms (*i.e.*, in the linear part of the NOE build- up curve).

Circular Dichroism. CD measurements were carried out at 25 °C on a Jasco J-1500 CD spectrometer (JASCO, Mary's Court Easton, MD, USA) using a Hellma quartz cuvette with an optical pathlength of 0.1 cm in methanol and PBS at pH 7.0. The spectra were obtained in the wavelength range from 180 to 260 nm and normalized to molar ellipticity per amino acid residue ($[\theta]\times10^{-3}$, deg × cm^2 × $dmol^{-1}$ × res^{-1}) using the exact peptide concentration obtained from their UV absorption at 280 nm.

Stability of Peptides in the Vitreous Fluid. For stability studies, 10 μM peptides were mixed with the porcine vitreous containing 1% antibiotics (penicillin/streptomycin; Gibco) in Eppendorf tubes. Each time point had a designated separate tube. The tubes were incubated at 37 °C, and the stability of the peptides in the vitreous environment was measured by monitoring their concentrations at different times, using ultra-performance liquid chromatography−tandem MS (UPLC−MS/MS).

Cytotoxicity Study. Cytotoxicity of the anti-VEGF peptides was evaluated using the MTT assay as previously described.[36] Briefly, the cells were seeded in 96-well plates at a density of 20,000 cells per well in 150 μL of the cell growth medium. After overnight incubation, the cells were washed with PBS. Peptides at various concentrations (0.01−100 μM) in the complete cell growth medium (100 μL) were added to each well for incubation (5 h at 37 °C, 7% CO_2). Poly-L- lysine-treated and untreated cells served as negative and positive controls, respectively. After incubation, the medium was aspirated, the cells were washed with PBS, and 150 μL of the growth medium was added to the cells. Then, the cells were washed with PBS after incubation for 24 h. A mixture of 90 μL of the complete growth medium and 10 μL of the 5 mg/ml MTT solution was added to the wells, and the plates were incubated for 4 h at 37 °C. After incubation, 100 μL of 10% sodium dodecyl sulfate (Merck) in 0.01 M HCl (Sigma-Aldrich) was added to the wells to solubilize formazan crystals, followed by overnight incubation at 37 °C. Formazan was quantified by measuring the absorbance at 570 nm using a spectral scanning multimode plate reader (Varioskan Flash, Thermo Scientific). Viability of the treated cells was compared to that of the untreated control cells.

VEGF-Binding Activity of the Peptides. The binding affinity of peptides with the VEGF was measured using MST.[37] The NanoTemper Monolith NT.115 Pico device (NanoTemper Tech- nologies GmbH, München, Germany), fluorescently labeled VEGF- RED protein with an initial concentration of 12 mM and Monolith NT.115 Premium capillaries, was used for the study. Binding of the label (NHS-RED) to the protein molecule (VEGF) was performed according to the standard protocol.[38] Interaction measurements were performed at a constant concentration of VEGF-RED (1 nM), varying the concentration of the anti-VEGF peptide in the range from 50 μM to 0.5 nM. The intensity of the infrared (IR) laser was adjusted automatically. The peptide−VEGF interaction was detected by studying the change in the fluorescence of the peptide−protein complex under the influence of an IR laser, which is proportional to the thermophoretic mobility of the labeled protein molecules. To calculate the resulting curve and the standard deviation, software MO Affinity Analysis from NanoTemper was used.

Inhibition of Cell Proliferation. HUVEC cells (VEGF-depend- ent cell line) were seeded in 96-well plates at a density of 25,000 cells per well in 200 μL of the cell growth medium containing recombinant human VEGF165 (0.5 ng/mL). After incubating the cells for 48 h, the growth medium was removed, and the cells were washed with PBS. The cells were incubated for another 24 h in the starvation medium (basal medium without VEGF and FBS). Anti-VEGF peptides in the concentration ranges 4, 20, 100, and 500 μM were pre-mixed with VEGF165 at a concentration of 50 ng/mL and incubated for 2 h at 37°C. After that, the cells were treated with the peptide and VEGF mixture solution for 48 h. Cells were washed with PBS, and the inhibition of proliferation was measured by an MTT assay. Data were expressed as percent proliferation (optical density of the sample/ optical density of the control without the peptide) and were fitted by PRISM to yield IC_{50} values for the peptides. Data are represented as mean±standard deviation (n = 3).

ACKNOWLEDGMENTS

This work was financially supported by Megagrant #14.W03.31.0025 of the Government of Russian Federation.

ABBREVIATIONS

Aib, *α*-aminoisobutyric acid; AMD, age-related macular degeneration; ARPE-19 cells, adult retinal pigment epithelial cell line-19; DCM, dichloromethane; DIPEA, *N*,*N*-diisopropy- lethylamine; DMF, *N*,*N*-dimethylformamide; EDT, ethanedi- thiol; FBS, fetal bovine serum; HATU, *N*-[(dimethylamino)-1*H*-1,2,3-triazolo-[4,5-*b*]pyridin-1-ylmethylene]-*N*-methylme- thanaminium hexafluorophosphate *N*-oxide; HBTU, *O*-(ben- zotriazol-1-yl)-*N*,*N*,*N*′,*N*′-tetramethyluronium hexafluorophos- phate; HPLC, high-performance liquid chromatography; HUVEC, human umbilical vein endothelial cell; MST, microscale thermophoresis; MeCN, acetonitrile; MTT, 3- (4,5-dimethylthiazol-2-yl)-2,5-diphenyltetrazolium bromide; NOESY, nuclear Overhauser effect spectroscopy; OxymaPure, ethyl (hydroxyimino)cyanoacetate; PBS, phosphate-buffered saline; TIS, triisopropylsilane; TFA, trifluoroacetic acid; UPLC−MS/MS, ultra-performance liquid chromatography− tandem mass spectrometry; VEGF, vascular endothelial growth factor; VEGFR, receptor for the vascular endothelial growth factor.

REFERENCES

(1) Markovic-Mueller, S.; Stuttfeld, E.; Asthana, M.; Weinert, T.; Bliven, S.; Goldie, K. N.; Kisko, K.; Capitani, G.; Ballmer-Hofer, K. Structure of the full-length VEGFR-1 extracellular domain in complex with VEGF-A. *Structure* 2017, *25*, 341−352.

(2) Carmeliet, P. Angiogenesis in health and disease. Nat. Med. 2003, 9, 653−660.

(3) Agarwal, A.; Rhoades, W. R.; Hanout, M.; Soliman, M. H.; Sarwar, S.; Sadiq, M. A.; Sepah, Y. J.; Do, D. V.; Nguyen, Q. D. Management of neovascular age-related macular degeneration. Current state-of-the-art care for optimizing visual outcomes and therapies in development. Clin. Ophthalmol. 2015, 9, 1001−1015.

(4) Wong, W. L.; Su, X.; Li, X.; Cheung, C. M. G.; Klein, R.; Cheng, C.-Y.; Wong, T. Y. Global prevalence of age-related macular degeneration and disease burden projection for 2020 and 2040: a systematic review and meta-analysis. Lancet Glob. Health 2014, 2, e106−e116.

(5) Glade-Bender, J.; Kandel, J. J.; Yamashiro, D. J. VEGF blocking therapy in the treatment of cancer. Expert Opin. Biol. Ther. 2003, 3, 263−276.

(6) Liang, X.; Xu, F.; Li, X.; Ma, C.; Zhang, Y.; Xu, W. VEGF signal system: The Application of antiangiogenesis. Curr. Med. Chem. 2014, 21, 894−910.

(7) Supuran, C. T. Agents for the prevention and treatment of age- related macular degeneration and macular edema: a literature and patent review. Expert Opin. Ther. Pat. 2019, 29, 761−767.

(8) Holash, J.; Davis, S.; Papadopoulos, N.; Croll, S. D.; Ho, L.; Russell, M.; Boland, P.; Leidich, R.; Hylton, D.; Burova, E.; Ioffe, E.; Huang, T.; Radziejewski, C.; Bailey, K.; Fandl, J. P.; Daly, T.; Wiegand, S. J.; Yancopoulos, G. D.; Rudge, J. S. VEGF-Trap: A VEGF blocker with potent antitumor effects. Proc. Natl. Acad. Sci. U.S.A. 2002, 99, 11393−11398.

(9) Ghosh, J. G.; Nguyen, A. A.; Bigelow, C. E.; Poor, S.; Qiu, Y.; Rangaswamy, N.; Ornberg, R.; Jackson, B.; Mak, H.; Ezell, T.; Kenanova, V.; de la Cruz, E.; Carrion, A.; Etemad-Gilbertson, B.; Caro, R. G.; Zhu, K.; George, V.; Bai, J.; Sharma-Nahar, R.; Shen, S.; Wang, Y.; Subramanian, K. K.; Fassbender, E.; Maker, M.; Hanks, S.; Vrouvlianis, J.; Leehy, B.; Long, D.; Prentiss, M.; Kansara, V.; Jaffee, B.; Dryja, T. P.; Roguska, M. Long-acting protein drugs for the treatment of ocular diseases. Nat. Commun. 2017, 8, 14837.

(10) D'Andrea, L. D.; Del Gatto, A.; De Rosa, L.; Romanelli, A.; Pedone, C. Peptides targeting angiogenesis related growth factor receptors. Curr. Pharm. Des. 2009, 15, 2414−2429.

(11) Checco, J. W.; Gellman, S. H. Iterative nonproteinogenic residue incorporation yields α/β-peptides with a helix−loop−helix tertiary structure and high affinity for VEGF. ChemBioChem 2017, 18, 291−299.

(12) Fairbrother, W. J.; Christinger, H. W.; Cochran, A. G.; Fuh, G.; Keenan, C. J.; Quan, C.; Shriver, S. K.; Tom, J. Y. K.; Wells, J. A.; Cunningham, B. C. Novel peptides selected to bind vascular endothelial growth factor target the receptor-binding site. Biochemistry 1998, 37, 17754−17764.

(13) Fedorova, A.; Zobel, K.; Gill, H. S.; Ogasawara, A.; Flores, J. E.; Tinianow, J. N.; Vanderbilt, A. N.; Wu, P.; Meng, Y. G.; Williams, S.- P.; Wiesmann, C.; Murray, J.; Marik, J.; Deshayes, K. The development of peptide-based tools for the analysis of angiogenesis. Chem. Biol. 2011, 18, 839−845.

(14) Haase, H. S.; Peterson-Kaufman, K. J.; Lan Levengood, S. K.; Checco, J. W.; Murphy, W. L.; Gellman, S. H. Extending foldamer design beyond α-helix mimicry α/β-peptide inhibitors of vascular endothelial growth factor signaling. J. Am. Chem. Soc. 2012, 134, 7652−7655.

(15) Reille-Seroussi, M.; Gaucher, J.-F.; Desole, C.; Gagey-Eilstein, N.; Brachet, F.; Broutin, I.; Vidal, M.; Broussy, S. Vascular endothelial growth factor peptide ligands explored by competition assay and isothermal titration calorimetry. Biochemistry 2015, 54, 5147−5156.

(16) Toniolo, C.; Crisma, M.; Formaggio, F.; Peggion, C. Control of peptide conformation by the Thorpe−Ingold effect (Cα-tetrasub- stitution). Biopolymers 2001, 60, 396−419.

(17) Yasutomi, S.; Morita, T.; Imanishi, Y.; Kimura, S. A molecular photodiode system that can switch photocurrent direction. Science 2004, 304, 1944−1947.

(18) Guryanov, I.; Moretto, A.; Campestrini, S.; Broxterman, Q. B.; Kaptein, B.; Peggion, C.; Formaggio, F.; Toniolo, C. Turn and helical peptide spacers: Combined distance and angular dependencies in the exciton-coupled circular dichroism of intramolecularly interacting bis- porphyrins. *Biopolymers* 2006, *82*, 482−490.

(19) Boal, A. K.; Guryanov, I.; Moretto, A.; Crisma, M.; Lanni, E. L.; Toniolo, C.; Grubbs, R. H.; O'Leary, D. J. Facile and E-selective intramolecular ring-closing metathesis reactions in 3(10)-helical peptides: A 3D structural study. *J. Am. Chem. Soc.* 2007, *129*, 6986−6987.

(20) Gatto, E.; Porchetta, A.; Stella, L.; Guryanov, I.; Formaggio, F.; Toniolo, C.; Kaptein, B.; Broxterman, Q. B.; Venanzi, M. Conformational effects on the electron-transfer efficiency in peptide foldamers based on alpha,alpha-disubstituted glycyl residues. *Chem. Biodiversity* 2008, *5*, 1263−1278.

(21) Becucci, L.; Guryanov, I.; Maran, F.; Guidelli, R. Effect of a strong interfacial electric field on the orientation of the dipole moment of thiolated Aib-oligopeptides tethered to mercury on either the N- or C-Terminus. *J. Am. Chem. Soc.* 2010, *132*, 6194−6204.

(22) Lau, J.; Bloch, P.; Schäffer, L.; Pettersson, I.; Spetzler, J.; Kofoed, J.; Madsen, K.; Knudsen, L. B.; McGuire, J.; Steensgaard, D. B.; Strauss, H. M.; Gram, D. X.; Knudsen, S. M.; Nielsen, F. S.; Thygesen, P.; Reedtz-Runge, S.; Kruse, T. Discovery of the once- weekly glucagon-like peptide-1 (GLP-1) analogue semaglutide. *J. Med. Chem.* 2015, *58*, 7370−7380.

(23) Varela, A.; Chouinard, L.; Lesage, E.; Smith, S. Y.; Hattersley, G. One year of abaloparatide, a selective activator of the PTH1 receptor, increased bone formation and bone mass in osteopenic ovariectomized rats without increasing bone resorption. *J. Bone Miner. Res.* 2017, *32*, 24−33.

(24) Pan, B.; Li, B.; Russell, S. J.; Tom, J. Y. K.; Cochran, A. G.; Fairbrother, W. J. Solution structure of a phage-derived peptide antagonist in complex with vascular endothelial growth factor. *J. Mol. Biol.* 2002, *316*, 769−787.

(25) Guryanov, I.; Cipriani, S.; Fiorucci, S.; Zashikhina, N.; Marchiano, S.; Scarpelli, P.; Korzhikov-Vlakh, V.; Popova, E.; Korzhikova-Vlakh, E.; Biondi, B.; Formaggio, F.; Tennikova, T. Nanotraps with biomimetic surface as decoys for chemokines. *Nanomedicine* 2017, *13*, 2575−2585.

(26) Byun, B. J.; Song, I. K.; Chung, Y. J.; Ryu, K. H.; Kang, Y. K. Conformational preferences of X-Pro sequences: Ala-Pro and Aib-Pro motifs. *J. Phys. Chem. B* 2010, *114*, 14077−14086.

(27) Karle, I. L.; Flippen-Anderson, J. L.; Uma, K.; Balaram, H.; Balaram, P. Peptide design: influence of a guest Aib-Pro segment on the stereochemistry of an oligo-Val sequence-solution conformations and crystal structure of Boc-$(Val)_2$-Aib-Pro-$(Val)_3$-OMe. *Biopolymers* 1990, *29*, 1433−1442.

(28) Gerig, J. T.; McLeod, R. S. Attempted synthesis of 2- methylalanyl-L-prolyl-L-tryptophan. An unexpected result. *J. Org. Chem.* 1976, *41*, 1653−1655.

(29) Subirós-Funosas, R.; El-Faham, A.; Albericio, F. Use of Oxyma as pH modulatory agent to be used in the prevention of base-driven side reactions and its effect on 2-chlorotrityl chloride resin. *Biopolymers* 2012, *98*, 89−97.

(30) Greenfield, N. J. Using circular dichroism spectra to estimate protein secondary structure. *Nat. Protoc.* 2006, *1*, 2876−2890.

(31) Hwang, T. L.; Shaka, A. J. Water suppression that works. Excitation sculpting using arbitrary wave-forms and pulsed-field gradients. *J. Magn. Reson., Ser. A* 1995, *112*, 275−279.

(32) Rance, M.; Sørensen, O. W.; Bodenhausen, G.; Wagner, G.; Ernst, R. R.; Wüthrich, K. Improved spectral resolution in COSY 1H NMR spectra of proteins via double quantum filtering. *Biochem. Biophys. Res. Commun.* 1983, *117*, 479−485.

(33) Bax, A.; Davis, D. G. MLEV-17-based two-dimensional homonuclear magnetization transfer spectroscopy. *J. Magn. Reson.* 1985, *65*, 355−360.

(34) Griesinger, C.; Otting, G.; Wuethrich, K.; Ernst, R. R. Clean TOCSY for proton spin system identification in macromolecules. *J. Am. Chem. Soc.* 1988, *110*, 7870−7872.

(35) Wüthrich, K. *NMR of Proteins and Nucleic Acids*; Wiley: New York, 1986.

(36) Mosmann, T. Rapid colorimetric assay for cellular growth and survival: application to proliferation and cytotoxicity assays. *J. Immunol. Methods* 1983, *65*, 55−63.

(37) Wienken, C. J.; Baaske, P.; Rothbauer, U.; Braun, D.; Duhr, S. Protein-binding assays in biological liquids using microscale thermophoresis. *Nat. Commun.* 2010, *1*, 100.

(38) Jerabek-Willemsen, M.; Wienken, C. J.; Braun, D.; Baaske, P.; Duhr, S. thermophoresis *Assay Drug Dev. Technol.* 2011, *9*, 342−353.